Determination of Optimal Timing for Non-Invasive Prenatal Testing and Robustness Analysis of Errors Based on Multi-Objective Optimization and K-Means Clustering

Yueran Ma [#, *], Sui Liang [#]

School of Mathematics and Computational Science, Xiangtan University, Xiangtan, China, 411100

* Corresponding Author Email: 202305755604@smail.xtu.edu.cn

[#]These authors contributed equally.

Abstract. This study addresses the challenge of determining the optimal timing for non-invasive prenatal testing (NIPT) based on BMI grouping. It aims to identify the optimal NIPT testing window for different pregnant women populations to minimize potential risks and maximize the pass rate for Y chromosome concentration. First, to eliminate subjective bias and uncover potential associations between BMI and test performance, virtual data were generated via Monte Carlo simulation to compensate for sparse real samples. Combined with the K-means elbow point method, pregnant women carrying male fetuses were grouped into four BMI intervals: [20.0, 25.7), [25.7, 32.2), [32.2, 39.4), and [39.4, 47.0). Second, a segmented sigmoid function was constructed to quantitatively define maternal potential risk, aligning with clinical risk trends. This function exhibits a three-stage progression: “initial slow growth,” “rapid growth,” and “extremely slow growth.” Subsequently, a multi-objective optimization model was established to minimize potential risk while maximizing Y chromosome concentration compliance rates. Solving this model using the NSGA-II algorithm yielded optimal NIPT timing points of 11.21, 12.69, 14.25, and 15.83 weeks for each BMI interval. Finally, error analysis revealed that detection errors significantly amplify false-negative risks in high-BMI and early-pregnancy-week cases, markedly narrowing the feasible testing window.

Keywords: K-means elbow point method, Multi-objective Optimization model, NSGA-II algorithm.

1. Introduction

Non-invasive prenatal testing (NIPT) effectively screens for fetal chromosomal abnormalities by analyzing fetal cell-free DNA in maternal peripheral blood, offering non-invasive, low-risk, and high-accuracy advantages [1-2]. Y-chromosome concentration in male fetuses serves as a critical indicator of fetal health, with its detection accuracy significantly influenced by maternal body mass index (BMI) and gestational age. Typically, NIPT testing can be performed between 10 and 25 weeks of gestation [3]. However, due to substantial individual variation among pregnant women, a uniform testing window cannot guarantee optimal outcomes. Therefore, determining the optimal NIPT testing time point based on different BMI groups to ensure detection accuracy and reduce potential risks is a current research priority. Previous studies often relied on simplistic BMI grouping or single-factor analysis, lacking comprehensive consideration of multiple factors and precise quantification of testing failure risks. This paper innovates by first employing Monte Carlo simulation to address sparse real-world data and utilizing K-means elbow point analysis to achieve data-driven, reasonable BMI grouping; Second, it constructs a segmented sigmoid function aligned with clinical progression characteristics to quantify potential risk. It innovatively abstracts timing selection into a multi-objective optimization problem minimizing potential risk while maximizing success rate, solving it with the NSGA-II algorithm to provide a Pareto optimal solution set for personalized clinical decision-making [4-6].

2. BMI Grouping Problem

2.1. Construction of Virtual Data Based on Monte Carlo Simulation

Due to the small number of samples with fetal Y-chromosome concentration close to the 4% threshold in the original data, it is difficult to accurately infer the earliest compliance time points under different BMI conditions using empirical data directly [7-8]. Therefore, combined with the nonlinear mixed-effects relationship model established, the Monte Carlo simulation method is used to simulate pregnant women with male fetuses and construct virtual data to make up for data sparsity. The specific steps are as follows:

Randomly generate virtual samples: Uniform random sampling is performed within the BMI range [20, 47] to generate 1000 virtual pregnant women, ensuring coverage of samples in each BMI interval.

Solve for compliance time points: For each virtual BMI value, based on the nonlinear mixed-effects relationship model, the numerical solver fsolve is called with four different initial values (10, 20, 30, 40 weeks) to solve the equation "Y-chromosome concentration = 0.04".

Screening of valid solutions: If the solution converges and falls within the reasonable pregnancy range (0–50 weeks), it is determined as a valid solution and retained; otherwise, it is discarded.

Determine the earliest compliance week: The minimum value among all valid solutions for each BMI value is taken and defined as the "earliest compliance week" under that BMI condition.

Construct the analysis dataset: Finally, two arrays of equal length are obtained: the BMI values of virtual pregnant women and the corresponding earliest compliance weeks, which are used for subsequent BMI grouping and optimization analysis of the optimal detection time point [9-10].

2.2. BMI Grouping Based on K-means Elbow Method

Using the K-means elbow method to group BMI can not only avoid the bias of subjective grouping but also explore the potential correlation between BMI and detection performance through a data-driven approach, providing a hierarchical basis for the subsequent risk assessment model. The specific steps are as follows:

BMI data preprocessing: Extract the BMI variable from the male fetus NIPT dataset (denoted as dataset $X = \{x_1, x_2, \dots, x_n\}$, where n is the sample size and x_i is the BMI value of the i-th pregnant woman); winsorize outliers to the range $[Q_1 - 1.5IQR, Q_3 + 1.5IQR]$ based on the IQR criterion to eliminate extreme interference; standardize the data scale using Z-score:

$$x_i' = \frac{x_i - \mu}{\sigma} \tag{1}$$

Where μ is the mean value of BMI and σ is the standard deviation. After standardization, the data follows a normal distribution with a mean of 0 and a variance of 1.

Configuration and execution of K-means clustering parameters: Set the K search range to 2, ..., 8 (the upper limit is 6 when $n < 200$); use Euclidean distance, k-means++ initialization, and a convergence threshold of 10^{-4}; run each K independently 20 times, select the result with the smallest SSE. The formula for calculating SSE is:

$$SSE(K) = \sum_{k=1}^{K} \sum_{x \in C_k} \|x - \mu_k\|^2 \tag{2}$$

Where C_k is the k-th cluster and μ_k is the center vector of the cluster.

Determination of the optimal K value: Draw the SSE-K line chart, visually locate the "elbow inflection point". If the inflection point is vague, use the second derivative method for quantitative identification and take the position with the largest absolute value; verify the consistency between the cluster mean and clinical BMI standards.

Verification of grouping results: Calculate the silhouette coefficient; a mean value > 0.5 indicates good grouping compactness; use ANOVA to test the differences in Y-chromosome concentration

among different BMI groups; a P-value < 0.05 indicates clinical significance; if the standards are not met, adjust the K value and re-cluster.

In the process of determining the optimal K value using the K-means elbow method, the inflection point is identified by combining visual positioning and the second derivative method. Figure 1 shows the graph of determining the optimal number of clusters using the elbow method, and the red dashed line at $K = 4$ is the finally determined inflection point.

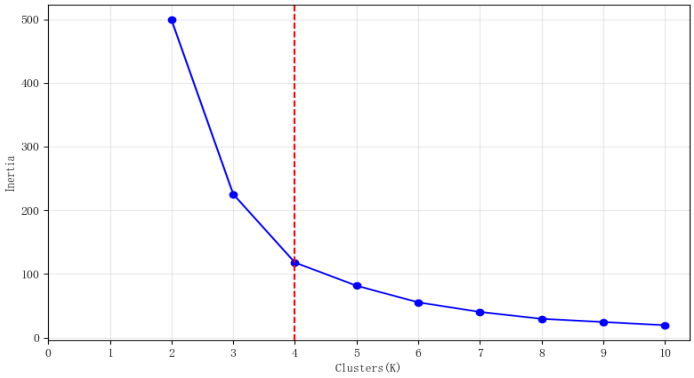

Figure 1. Graph of determining the optimal number of clusters using the elbow method.

2.3. Results of BMI Grouping Problem

Through Monte Carlo simulation + K-means elbow method, the final clustering results are shown in Table 1. The BMI grouping of pregnant women with male fetuses is: [20.0, 25.7), [25.7, 32.2), [32.2, 39.4), [39.4, 47.0]. Clustering results of K-means elbow method is shown in table 1.

Table 1 Clustering results of K-means elbow method.

Cluster	Average BMI	Number of Samples	BMI Range
1	22.8	231	20.1–25.6
2	28.9	230	25.7–32.1
3	35.7	266	32.2–39.3
4	43.3	273	39.4–47.0

3. Determination of the Optimal NIPT Time Point

3.1. Quantitative Definition of Pregnant Women's Potential Risks

Based on the description in the problem that the risk of early detection within 12 weeks is low, the risk of detection in the middle stage (13–27 weeks) is high, and the risk of late detection after 28 weeks is extremely high, a piecewise Sigmoid function is constructed.

The corresponding relationship between the number of gestational weeks t and the potential risk f is defined as shown in Table 2:

Table 2 Corresponding relationship between the number of gestational weeks and potential risks.

Gestational Weeks t	10	11	12	18	25	26	27
Risk f	0.1	0.15	0.2	0.4	0.7	0.85	1

Among them, a potential risk $f \in [0,0.2)$ indicates a relatively low potential risk, $f \in [0.2,0.7)$ indicates a high potential risk, $f \in [0.7,1)$ indicates that the potential risk is between high and extremely high, and $f = 1$ indicates an extremely high potential risk.

The function needs to satisfy the three-stage trend of "initial slow period", "rapid rise period", and "saturation approaching period". At the same time, the function values at the boundary points ($t = 12$, $t = 25$) are continuous without jumps, and $f(t) \to 1$ (risk converges to the threshold) when $t \to 27^{+}$.

3.1.1. Slow growth stage ($t \in [10, 12]$)

This stage corresponds to the early stage of NIPT (gestational weeks < 12). The fetal Y-chromosome concentration is low, and the potential risk decreases slowly. A low-slope Sigmoid function needs to be used for fitting:

$$f_1(t) = \frac{a}{1 + e^{k_1 \times (t-11)}} \tag{3}$$

Where the amplitude parameter a matches the index increase in this stage and reserves fitting redundancy; the absolute value of the slope parameter k_1 is large, which needs to fit the "slow growth" characteristic; the inflection point $t = 11$ is located at the midpoint of this stage to ensure the symmetric trend of 10–12 weeks and avoid endpoint fitting deviation.

3.1.2. Rapid growth stage ($t \in (12, 25)$)

This stage is the golden detection period of NIPT. The Y-chromosome concentration increases rapidly, and the potential risk decreases significantly. A medium-slope Sigmoid function with a reasonable inflection point needs to be used to adapt to the growth rate change of "first fast then slow":

$$f_2(t) = a + \frac{b - a}{1 + e^{-k_2 \times (t-18.5)}} \tag{4}$$

Where the amplitude parameter $(b - a)$ covers the index increase in this stage to meet the demand for rapid growth; the absolute value of the slope parameter k_2 should be moderate; the inflection point $t = 18.5$ corresponds to the key gestational week of "a sharp increase in the Y-chromosome concentration compliance rate", ensuring that the trend is consistent with the biological mechanism.

3.1.3. Very slow growth stage ($t \in (25, 27]$)

In this stage, the Y-chromosome concentration has reached the standard stably, and the potential risk is close to the clinical threshold. A high-slope saturated Sigmoid function needs to be used to fit the growth rate attenuation process. The function form is:

$$f_3(t) = b + \frac{1 - b}{1 + e^{-k_3 \times (t-26)}} \tag{5}$$

Where the amplitude parameter $(1 - b)$ matches the index increase in this stage to ensure that the function finally converges to 1; the absolute value of the slope parameter k_3 is large, making the curve enter the saturation period quickly and fitting the "very slow growth" characteristic; the inflection point $t = 26$ is located at the midpoint of this stage to ensure the continuous attenuation of the growth rate and avoid over-fitting at the end.

3.1.4. Consistency check

To ensure the physical continuity of the potential risk index, a consistency check is performed on the functions at the boundary points. When $t = 12$, $f_1(12) \approx 0.2$ and $f_2(12) \approx 0.2$, and the values match completely; when $t = 25$, $f_2(25) \approx 0.7$ and $f_3(25) = 0.7$, and the values match completely. It can be seen that there is no jump at the junction of the two stages, which is consistent with the gradual characteristics of risk changes.

3.1.5. Obtain the quantitative definition of the final potential risk

Comprehensive of the above construction and verification, the piecewise Sigmoid function definition of the potential risk-related index $f(t)$ is as follows:

$$f(t) = \begin{cases} \dfrac{a}{1 + e^{k_1 \times (t-11)}}, & 10 \le t \le 12 \\ a + \dfrac{b - a}{1 + e^{-k_2 \times (t-18.5)}}, & 12 << t \le 25 \\ b + \dfrac{1 - b}{1 + e^{-k_3 \times (t-26)}}, & 25 << t \le 27 \\ 1, & t > 27 \end{cases} \quad (6)$$

Where $f(t) \in [0.1,1]$, and a larger value indicates a higher potential risk of NIPT detection; $k_1 = 1.9629$, $k_2 = 0.3211$, $k_3 = 24.2163$; a and b are obtained by data fitting.

3.2. Establishment of the Risk Minimization Model

For each BMI group i ($i = 1,2, \dots, k$, where k is the total number of groups, 4) of pregnant women with male fetuses, a potential risk minimization model is established respectively. Let T_i be the NIPT time point of the i-th group, that is, NIPT is performed at T_i for the i-th group.

To ensure that all pregnant women undergo detection as early as possible without false negatives caused by too early detection, the time point of NIPT is constrained to be within the detection period. Thus, the constraint condition is obtained:

$$10 \le T_i \le 25 \quad (7)$$

Based on the goal of minimizing the potential risk of pregnant women, the objective function corresponding to the i-th group is established:

$$\min f(T_i) \quad (8)$$

In actual detection, in addition to minimizing the potential risk, there is an implicit condition of making the detection as accurate as possible. However, it is difficult to ensure the accuracy of the results when the Y-chromosome concentration of male fetuses is less than 4%. Therefore, the proportion of fetal chromosome concentration that meets the standard should be as high as possible. Thus, the second objective function is obtained:

$$\max P(Y \ge 4\%) \quad (9)$$

In summary, a multi-objective programming model for minimizing potential risks + maximizing the Y-chromosome concentration compliance rate is obtained:

$$\min f(T_i) \quad (10)$$

$$\max P(Y \ge 4\%) \quad (11)$$

$$s.t.\ 10 \le T_i \le 25 \quad (12)$$

Where $f(T_i)$ is the piecewise Sigmoid function defined in the previous subsection, and $i = 1,2, \dots, k$ correspond to k BMI subgroups respectively.

3.3. Solution of the Risk Minimization Model

The NSGA-II algorithm, an improved genetic algorithm, can automatically find a series of balanced solutions (Pareto frontier) between the two mutually exclusive goals of "reducing risks" and "increasing compliance rates". It is particularly suitable for this complex, non-convex multi-objective optimization with Monte Carlo noise. The NSGA-II algorithm is used to solve this multi-objective programming model, and the specific steps are shown in Figure 2.

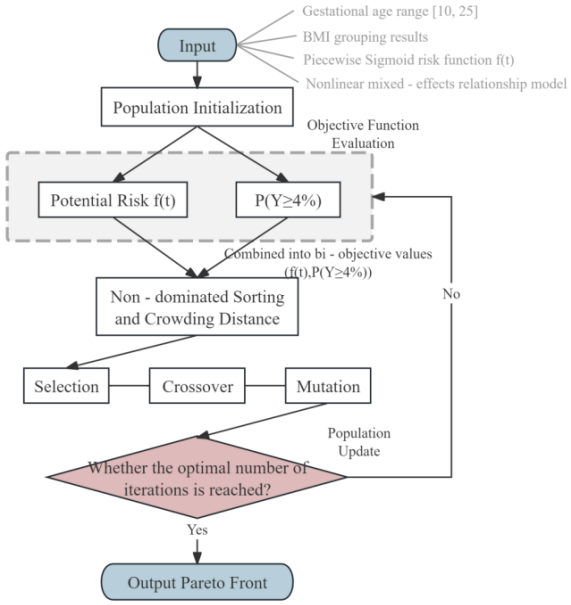

Figure 2. Flow chart of the NSGA-II algorithm for solving the risk minimization problem.

Problem modeling: Take the gestational weeks $t \in [10,25]$ as the decision variable, set the first objective to minimize the potential risk $f(t)$, the second objective to maximize the compliance rate $P(Y \geq 4\%)$, and convert it to minimizing $-P(Y \geq 4\%)$.

Population initialization: Randomly generate candidate solutions of gestational weeks within the constraint interval to form the initial population.

Objective function evaluation: Calculate $f(t)$ and $-P(Y \geq 4\%)$ for each individual to obtain dual objective values.

Non-dominated sorting and crowding degree: Sort the individuals according to Pareto optimality and calculate the crowding distance to maintain the diversity of the solution set.

Selection and evolution operations: Adopt tournament selection and generate new solutions through simulated binary crossover and polynomial mutation to ensure that the interval constraints are met.

Population update: Merge the parent and offspring populations, repeat non-dominated sorting and crowding degree calculation, and screen out a new generation of populations with a fixed size.

Termination and output: Iterate until the set number of generations is reached, output the Pareto optimal solution set, and select the best compromise solution based on the ideal point distance to determine the recommended detection time point.

3.4. Results of Determining the Optimal NIPT Time Point

The optimal NIPT time points and the corresponding values of the two objective functions for each interval obtained by solving with the NSGA-II algorithm are shown in Table 3. It can be seen from the table that the optimal NIPT time point for the BMI interval [20.0, 25.7) is the 11.21st week, approximately 11 weeks and 1 day; for [25.7, 32.2), it is the 12.69th week, approximately 12 weeks and 5 days; for [32.2, 39.4), it is the 14.25th week, approximately 14 weeks and 2 days; for [39.4, 47.0], it is the 15.83rd week, approximately 15 weeks and 6 days. Optimal NIPT time points for each interval are shwon in table 3.

Table 3. Optimal NIPT time points for each interval.

BMI Interval	Optimal NIPT Time Point (Weeks)	Risk Value	Detection Success Rate
20.0–25.7	11.21	0.1482	1.0000
25.7–32.2	12.69	0.2579	1.0000
32.2–39.4	14.25	0.2921	0.9130
39.4–47.0	15.83	0.3410	0.2905

3.5. Analysis of the Impact of Detection Errors on Results

To systematically evaluate the impact of detection errors on the optimal NIPT time point results, the analysis is carried out from the following three dimensions.

3.5.1. Identification of high-risk areas and error amplification effects

By conducting Monte Carlo simulations point by point on the gestational week-BMI grid, the false negative rate heatmap under different measurement error levels is calculated and drawn to identify high-risk areas. The false negative risk heatmap is shown in Figure 3.

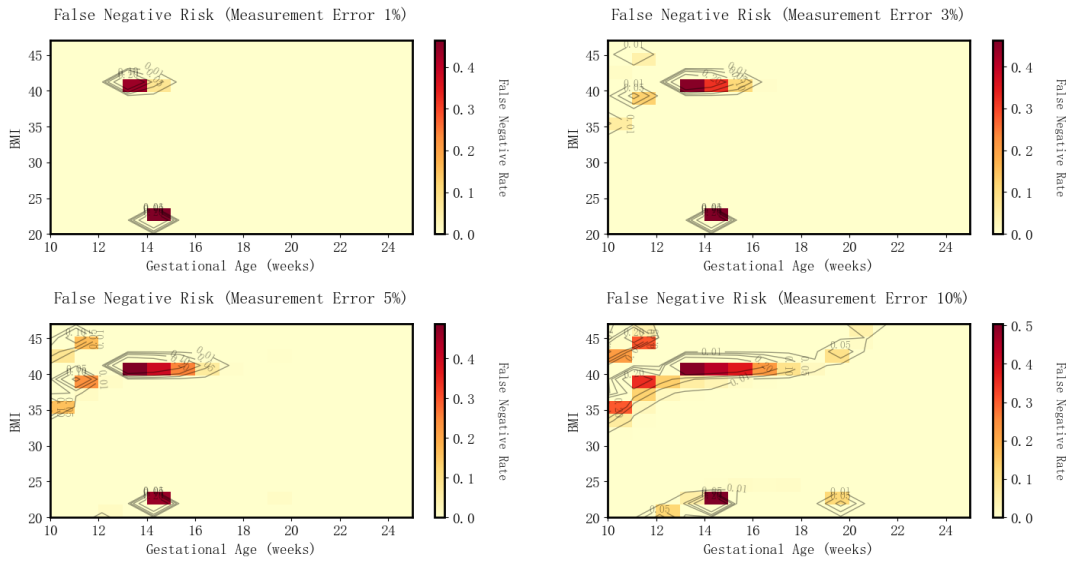

Figure 3. False negative risk heatmap.

The results show that detection errors will significantly amplify the risk in specific BMI and gestational week combination areas. When the measurement error reaches 10%, the false negative rate of people with BMI 40–45 and gestational weeks 10–15 exceeds 40%, becoming the highest risk area; people with BMI 35–40 and gestational weeks 18–22 is in the medium-risk area, with a false negative rate of 20%–30%. It can be seen that people with high BMI is particularly sensitive to measurement errors, and an increase in the error level will cause a non-linear increase in the false negative rate, thereby delaying the optimal time for clinical intervention.

3.5.2. Reliability differences among different BMI groups

The reliability data of all gestational weeks correspond to a fixed BMI value is obtained, and a curve of reliability changing with gestational weeks is drawn. The response differences among different BMI groups are revealed by comparing the curve characteristics of different BMI groups. The reliability comparison results under different BMI values are shown in Figure 4.

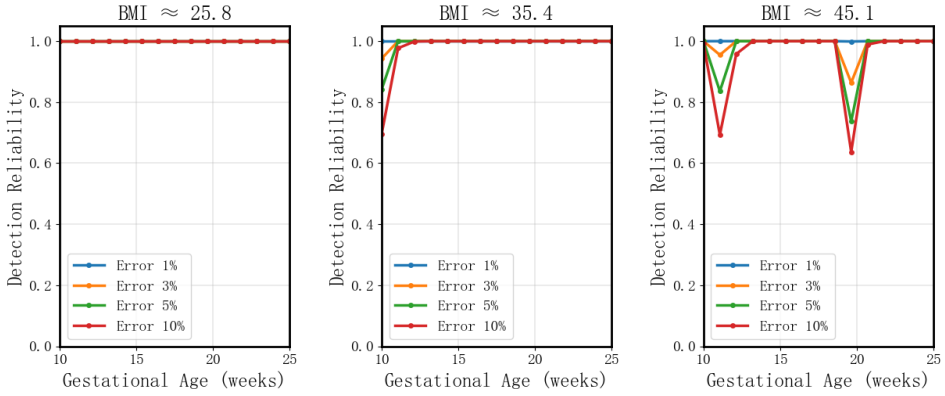

Figure 4. Reliability comparison under different BMI values.

There are significant heterogeneities in the impact of errors on detection reliability among different BMI groups. The low BMI group (≈25.8) has a reliability close to 100% throughout the gestational week range and is hardly affected by errors; the medium BMI group (≈35.4) experiences a sharp drop in reliability at 10–11 weeks of gestation, which is only 70% under a 10% error; the high BMI group (≈45.1) shows a double trough characteristic (11 weeks and 20 weeks of gestation), with the lowest reliability dropping to 65%. This indicates that in people with medium and high BMI, errors have a particularly significant impact on early and mid-term detection, and specific gestational weeks should be avoided to ensure detection effectiveness.

3.5.3. Contraction of the optimal detection window and stratification of error tolerance

For each BMI value, find all gestational weeks with reliability exceeding the threshold (e.g., 95%), and take the minimum and maximum values as the detection window boundaries under that BMI. The contraction mode is displayed by visualizing the windows under different error levels. The analysis results of the optimal detection window are shown in Figure 5.

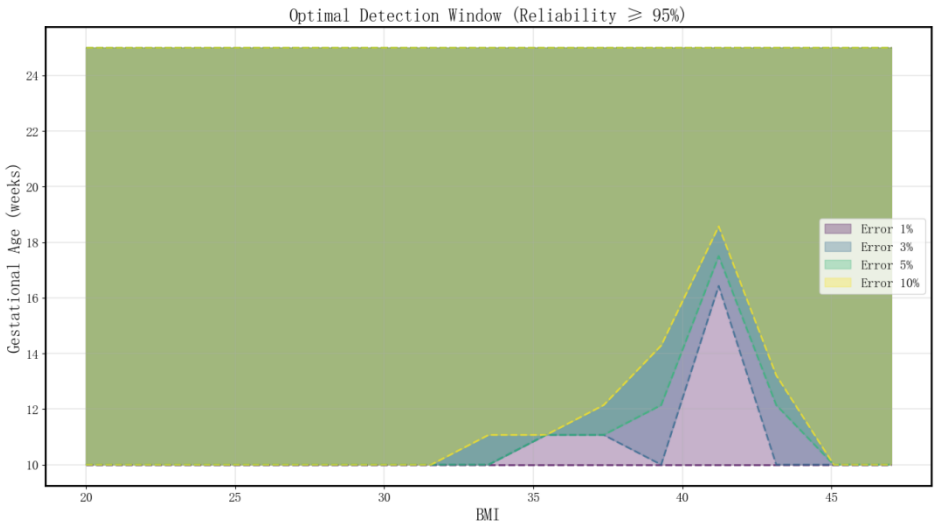

Figure 5. Analysis of the optimal detection window.

With the increase in the error level, the detection window with reliability (≥95%) shows an obvious "triangular contraction" characteristic. Under a 1% error, the detection window almost covers the entire range (BMI < 42, 10–18 weeks of gestation); when the error increases to 10%, the reliable window shrinks significantly, limited to the narrow area of BMI < 40 and 11–16 weeks of gestation. It can be seen that measurement errors directly limit the flexibility and scope of application of detection. In a high-error environment, only the central area is clinically feasible.

In summary, detection errors have a significant impact on the reliability of NIPT results, especially in people with high BMI and early gestational weeks. Errors not only amplify the false negative risk but also aggravate the reliability differentiation among groups and lead to a significant reduction in the feasible detection window, thereby increasing clinical risks. Therefore, in practical applications, it is necessary to strictly control measurement errors and dynamically adjust the detection time point based on BMI stratification and error levels to maximize the accuracy and clinical safety of the results.

4. Conclusions

This study successfully developed a framework integrating K-means clustering with multi-objective optimization to determine the optimal timing for non-invasive prenatal testing (NIPT) across different BMI categories of pregnant women. Results indicate that the optimal testing window should be correspondingly delayed as maternal BMI increases. The study provides specific optimal time points for four BMI intervals: [20.0, 25.7), [25.7, 32.2), [32.2, 39.4), and [39.4, 47.0]) with specific optimal time points (11.21, 12.69, 14.25, and 15.83 weeks, respectively). Error analysis

further indicates that detection errors significantly amplify the risk of false negatives in high-BMI and early-gestational-age cases, narrowing the reliable testing window.

Despite these achievements, the model retains limitations. For instance, the nonlinear mixed-effects model primarily focuses on gestational age and BMI as core variables, neglecting other potential factors like hormone levels, lifestyle, and genetic background, which may restrict its comprehensiveness. Additionally, within the complex optimization algorithm, there remains room for improvement in risk coefficient calibration and model interpretability. Looking ahead, the nonlinear mixed-effects modeling approach developed in this study can be extended to other prenatal screening programs for analyzing changes in fetal biomarker concentrations. Furthermore, the optimization framework combining Monte Carlo simulation with the NSGA-II algorithm holds broad applicability for addressing other medical screening and public health decision-making problems involving multiple factors and objectives.

References

[1] Ju Aiping, Meng Xiangrong, Qin Yanling, et al. Application Value of Non-Invasive Prenatal Testing in Screening Fetal Chromosomal Copy Number Variations [J]. Practical Electrocardiography and Clinical Diagnosis and Treatment, 2025, 34(05): 665-671.

[2] Zhu Sijing, Zhen Shuai, Niu Hui, et al. Current Status and Future Prospects of Whole Exome Sequencing in Prenatal Diagnosis [J]. Chinese Journal of Maternal and Child Health Research, 2025, 36(09): 61-67.

[3] Shi Weihui, Xu Chenming. Application Value of Non-Invasive Prenatal Testing in Diagnosing Obstetric Maternal Complications and Comorbidities [J]. Journal of Practical Obstetrics and Gynecology, 2025, 41(08): 617-620.

[4] Zhou Jing, Ji Xiuqing, Li Li, et al. Analysis of Seven Cases of Y Chromosome Abnormalities in Amniotic Fluid Cells Detected by Prenatal Diagnosis [J]. International Journal of Obstetrics and Gynecology, 2025, 52(04): 394-401.

[5] Jiang Liyia, Lu Shaokan, Du Jia'en, et al. Development and Application of Non-Invasive Prenatal Testing Technology [J]. Clinical Medical Research and Practice, 2025, 10(23): 191-194.

[6] Zhang Peng, Mo Weiying, Meng Minghui, et al. Impact of Non-Invasive Prenatal Testing on Detection of Sex Chromosome Aneuploidy and Related Ethical Considerations [J]. Chinese Journal of Clinical Medicine, 2025, 18(06): 690-695.

[7] Zhang Yumei, Han Ying, Qiu Huiguo. Application Value of Non-Invasive Prenatal Screening Technology in Detecting Chromosomal Abnormalities and Microdeletions [J]. Journal of Yanbian University of Science and Technology (Medical Science), 2025, 48(06): 59-61.

[8] Huang Chunyuan, Xu Xueqing, Shao Congwen. A Reassuring “Birth Plan” for Your Baby: Non-Invasive Prenatal Testing and Scientific Reproductive Guidance After Miscarriage [C]//Guangdong Tumor Rehabilitation Association. 2025 South China Health Management Forum Health Science Popularization Collection. Precision Medicine Clinical Laboratory, Shenzhen Hospital of Southern Medical University; 2025:315-317.

[9] Tan Lingjun, Wang Bin, Huang Zhiqiong, et al. Application of Expanded Non-Invasive Prenatal Testing in Prenatal Diagnosis in Plateau Regions [J]. Chinese Journal of Prenatal Diagnosis (Electronic Edition), 2025, 17(02):7-12.

[10] Jiang Yulin. Unexpected Findings in Non-Invasive Aneuploidy Screening: To Report or Not to Report? [J]. Chinese Journal of Prenatal Diagnosis (Electronic Edition), 2025, 17(02):12.